Transition between coalescence and bouncing of droplets on a deep liquid pool

He Zhao[a,*], Amy Brunsvold[b], Svend Tollak Munkejord[b]

[a]*Department of Energy and Process Engineering, Norwegian University of Science and Technology (NTNU), Kolbjørn Hejes vei 1B, NO-7491 Trondheim, Norway*
[b]*SINTEF Energy Research, Sem Sælands vei 11, NO-7465 Trondheim, Norway*

Abstract

This study focused on the bouncing of sub-millimetric droplets (below 0.7 mm) of three different fluids, distilled water, technical ethanol and 1-propanol on a deep liquid pool of the same fluids. Four different flow regimes including low-energy-collision coalescence, bouncing, high-energy-collision coalescence, and partial coalescence were observed in the experiments. These regimes were plotted in velocity-diameter diagrams, which showed that there was a diameter limit, $D \approx 0.2$ mm, above which the low-energy-collision coalescence was inhibited. The contact time, in which the impinging droplets and the liquid surface interacted in the bouncing process, was studied, and the results showed the same characteristic time scale of the contact time as those of Richard et al. (in Nature 417:811, 2002) and Thoroddsen and Takehara (in Phys Fluids 12 (6):1265–1267, 2000). The restitution coefficients for all fluids were investigated, and the water data agreed well with the values reported in the literature (Bach et al., J Fluid Mech 518:157–185, 2004; Jayaratne and Mason, Proc R Soc Lond A 280 (1383):545–565, 1964). Based on stable restitution coefficients, which varied with fluids, the effects from both viscosity and surface tension were discussed. Further, a correlation ($K = \mathrm{We} \cdot \mathrm{Oh}^{-0.58}$) was generalized to characterize the two transitions between coalescence (both high-energy- and low-energy-collision types) and bouncing, and a comparison with the model and data of Huang and Zhang (in Petrol Sci 5:62–66, 2008) showed that the generalized model characterized the coalescence-bouncing threshold well for the experimental fluids in the present study and oil with much higher viscosity.

Keywords: droplet, impact, bouncing, coalescence

1. Introduction

1.1. Motivation and background

The investigation of droplet impact phenomena can be traced back to 1876 when Worthington (1876) studied the "finger pattern" and the central jet formation. The impact of a droplet onto a wet/dry surface can lead to different outcomes, in which the droplet may splash with the

*Corresponding author. Tel.: +47-99306561; fax:+47-73593580
Email addresses: he.zhao@ntnu.no;hez@pvv.ntnu.no (He Zhao), amy.brunsvold@sintef.no (Amy Brunsvold), svend.t.munkejord@sintef.no (Svend Tollak Munkejord)

production of a central jet, coalesce, deposit, or rebound on the surface. A detailed understanding of droplet impacts can contribute to many fields, including spray cooling and coating processes (Aziz and Chandra, 2000; Pasandideh-Fard et al., 2001), optimization of internal combustion processes (Moita and Moreira, 2007), prevention of soil erosion (Ohnuki and Shimizu, 2004) and spreading of fungal pathogens (Madden, 1997), pesticides spraying processes (Tuck et al., 1997) etc.

The knowledge of droplet impact is critical for the gas-liquid separation processes, as the design and optimization of the gas-liquid separation equipment can be improved by understanding the droplet impact phenomena (Austrheim, 2006; Johnsen, 2007; Dorao et al., 2009). Bouncing of droplets on a surface can either be a disadvantageous or an advantageous phenomenon for industrial equipment. For heat exchangers in the liquefied natural gas (LNG) industry, the most effective heat transfer occurs with a thin liquid film covering the heat exchanger tubes. Bouncing of refrigerant droplets on dry heat exchanger tubes reduces the conduction heat transfer, while bouncing on film-covered tubes may keep the film-thickness in a desired range for the effective heat transfer. However, for recovery boilers in the pulping industry, bouncing of droplets is favored as it reduces the heat exchanger fouling formed of ash-deposit (Mao et al., 1997). In high-pressure (up to 100 bar) liquid-gas separation equipment, bouncing, leading to a decreased performance of the equipment, is seen as one of the dominant phenomena due to high gas density (Dupuy et al., 2010).

An understanding of the phenomena of bouncing and coalescence, especially the conditions at which bouncing transits to coalescence, can lead to an enhancement of the flow conditions, i.e. the efficiency, of the equipment, and moreover, the boundary conditions for distinguishing different flow regimes can be used for developing numerical models, which can be used for equipment design.

1.2. Literature review

Regarding droplet-film impact, according to Pan and Law (2007), as the Weber number (We $= \frac{\rho D V^2}{\sigma}$, showing the relative importance of inertia to surface tension, with ρ, D, V and σ denoting density, diameter, velocity and surface tension) of the impinging droplet increases, there exist four different regimes: (a) low-energy-collision coalescence, (b) bouncing, (c) high-energy-collision coalescence and (d) splashing. Both types of coalescence are phenomenologically characterized by the merging of an impinging droplet into a liquid layer, and the difference between them is that the droplet deformation and surface waves are much weaker in the low-energy-collision coalescence due to low impinging kinetic energy. Bouncing and splashing are related with the rebound of the primary impinging droplet and the formation of secondary droplet, respectively.

The bouncing of droplets can occur on either a dry or a wetted surface. The investigations of bouncing on a dry surface supplied useful information for developing hydrophobic materials. Mao et al. (1997) used droplets of a mixture of water and sucrose with a diameter range of 1.5-3.5 mm to study the impact process, especially the droplet deformation on different dry surfaces. Richard and Quéré (2000); Clanet et al. (2004); Bartolo et al. (2006) studied the bouncing of water droplets in the millimetric range on highly hydrophobic surfaces, where the impinging kinetic energy can be well conserved during the impingement. These investigations focused on the bouncing process evolution, while Bartolo et al. (2006) also studied transitions between bouncing and non-bouncing regimes. In the recent years, more studies (Brunet et al., 2008; Jung and Bhushan, 2008; Rioboo et al., 2008; Deng et al., 2009; Jung and Bhushan, 2009; Tsai et al., 2009;

Kwon et al., 2011) were devoted to the investigation of drops impacting onto a nanostructured superhydrophobic surface. In these studies, the main interest was the discrimination of different impact regimes, especially the characterization of the impact ending states, Cassie-Baxter or Wenzel, which indicate nonwetting and wetting of the surface, respectively. Brunet et al. (2008) compared the wetting properties of surfaces with different nanowires with and without an electric field. Jung and Bhushan (2008) presented a study of the static contact angles for Cassie-Baxter and Wenzel states and the critical impinging velocity leading to the two states, and later, Jung and Bhushan (2009) included the effects from drop vibration. Rioboo et al. (2008) characterized thresholds using constant Weber numbers for different impact regimes such as splashing, jetting, deposition and rebound, and it was found also that the thresholds depended on the contact angle hysteresis. Deng et al. (2009) introduced an effective water-hammer pressure, which led to the Wenzel state, and based on both Laplace and water-hammer mechanisms, Kwon et al. (2011) characterized the threshold between Cassie-Baxter and Wenzel states for the gentle deposition by using droplet size. Employing the Weber and Reynolds number, Tsai et al. (2009) studied the transitions between different flow regimes with a varying surrounding pressure on different nanostructured surfaces.

Partial coalescence, as a transitional regime between coalescence and bouncing, was investigated by Thoroddsen and Takehara (2000); Blanchette and Bigioni (2006); Zhang et al. (2009). Among these investigations, Thoroddsen and Takehara (2000) observed successive partial coalescence resulted from one impinging droplet, and an impact time scale relating the density, diameter and surface tension was suggested. Blanchette and Bigioni (2006) studied the effect of viscosity during the partial coalescence. Zhang et al. (2009) looked into the partial coalescence as a result of drop-drop interaction, and the relation between the ratio of two parental droplets and the daughter-droplet was presented.

The investigations of bouncing droplets on a wetted surface generally focused more on the liquid side rather than on solid materials, such as the differences of phenomena and criteria for different liquids, and this was due to the fact that the substrate was less involved during the impingement. Transitions between different flow regimes were of great interest in those studies. Schotland (1960) looked into the transition between bouncing and high-energy-collision coalescence (B-C) of water, methanol and benzene droplets with a diameter range of 0.3–1 mm on a liquid surface, and the transition was characterized by either a dimensional parameter (critical falling height) or a non-dimensional parameter (Weber number). Jayaratne and Mason (1964) characterized the transition from low-energy-collision coalescence to bouncing (C-B) of water droplets ranging from 0.074 to 0.184 mm by using velocity and impact angle, and bouncing droplets were obtained from non-head-on impingement with impinging angles of 30–75°. Bach et al. (2004) used very small water droplets (diameter 0.04 and 0.08 mm) to study the effects from gas viscosity in the C-B transition, and it was found that rather than the Weber number, bouncing was much more sensitive to the gas viscosity. Both Jayaratne and Mason (1964) and Bach et al. (2004) reported the restitution coefficient around 0.2–0.3. Pan and Law (2007) investigated the B-C transition using tetradecane and dodecane droplets with diameters between 0.25 and 0.65 mm, and the Weber number was used to characterize the transition. Huang and Zhang (2008) presented a model to predict the transition between coalescence and bouncing.

Common features found in the literature on bouncing-coalescence were the limitation of experimental fluids, insufficient experiments with vertical impact, and the lack of generalized models, as well as verification of the existing models (Huang and Zhang, 2008). Distilled water was the only experimental fluid in many applications (Jayaratne and Mason, 1964; Richard and Quéré, 2000; Richard et al., 2002; Bach et al., 2004; Bartolo et al., 2006), and it was mainly

because water was the most commonly found fluid in nature and due to the application for hydrophobic materials. As a result, there was inadequate experimental data and validation using other fluid properties, and the effects of the physical properties of fluids were insufficiently discussed. Most of the above investigations of bouncing on a liquid film (Bach et al., 2004; Jayaratne and Mason, 1964; Schotland, 1960) used oblique impinging angles, which was a favorable condition for inhibiting coalescence due to the slowing-down of the drainage of the interfacial gas layer (Couder et al., 2005). Oblique impingement introduced a favorable condition for bouncing, but, in the sense of dimensional analysis, this complicated the study due to an increased number of degrees of freedom of the system (the tangential velocity vector of droplet). Thus, more uncertainties were brought into the analysis. The present investigation therefore concerns the transition between bouncing and coalescence with vertical droplet-pool impingement of three different fluids, distilled water, technical ethanol and 1-propanol. Both low- and high-energy-collision coalescence is covered.

The rest of this article is organized as follows: in Section 2, the experimental method is briefly reviewed, and Section 3 summarizes the experimental observations. The results, including the analysis of regime-transitions using dimensional and dimensionless parameters and the effects of viscosity and surface tension in the bouncing process, are discussed in Section 4. Section 5 concludes the article.

2. Experimental method

Bouncing and coalescing droplet-pool interactions of water, technical ethanol, and 1-propanol were investigated with high-speed visualization techniques. The physical properties of the experimental fluids are listed in Table 1. Technical ethanol was a solution of 98 wt% water-vapor-saturated ethanol mixed with 2 wt% methyl isobutyl ketone (MIBK) as an additive. Only an approximate density ($\approx 800\,\mathrm{kg/m^3}$) was given on the data sheet by the producer (Kemetyl Norge AS), thus density, surface tension (by a capillary method) and viscosity (by a Cannon-Fenske Routine Viscometer) were measured in laboratory.

Table 1: Physical properties of the experimental fluids at atmospheric pressure and 25°C.

Fluids	ρ ($\mathrm{kg/m^3}$)	μ ($\mathrm{mPa \cdot s}$)	σ ($\mathrm{mN/m}$)
Distilled water[1]	996.9	0.890	71.99
Technical ethanol[2]	805.8	1.367	22.41
1-propanol	799.6[1]	1.968[3]	23.28[4]

A schematic diagram of the apparatus used in the experiments is shown in Figure 1, and has been described in detail previously (Zhao, 2009; Zhao et al., 2010). In summary, the experimental setup consisted of a droplet generator and a deep liquid pool, and high-speed visualization, including backlight source and high-speed camera. These components will be described briefly.

[1] from Lide (2009).
[2] measured in our laboratory.
[3] from Tanaka et al. (1987).
[4] from Vaquez et al. (1995).

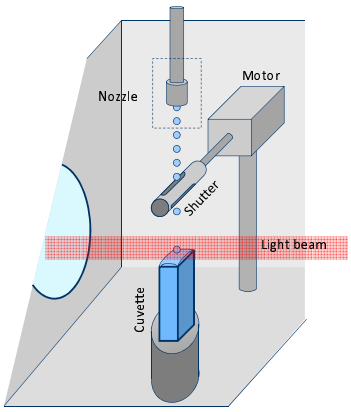

Figure 1: Schematic diagram of the experimental apparatus.

The droplet-pool interactions were illuminated with a collimated, white light, LED backlight and images of the phenomena were captured by a high-speed camera (Vision research, Phantom V9.1) mounted with a long-distance microscope and a close-focus lens. The resolution was 576×288 pixels, and the frame rate was 9216 frames per second (fps). The exposure time was from 5 to 10 μs.

A pinhole nozzle was used to generate a mono-dispersed stream of liquid droplets using the Plateau-Rayleigh instability (Lord Rayleigh, 1878, 1879), with droplet diameters and velocities adjusted via the pressure exerted on the liquid reservoir and the nozzle diameter. The experimentally obtained diameter and velocity ranges were 0.07–0.7 mm and 0.1–8 m/s, respectively. A shutter, or slotted disk, rotating 1000–10000 revolutions per minute, limited the impact frequency of the droplets. It was pointed out by Zhbankova and Kolpakov (1990) that an impinging frequency lower than 60 Hz was necessary for obtaining isolated impacts. In our investigation, most of the impinging frequencies were below 125 Hz[5], and in addition, isolated impacts were selected by inspection. A liquid-filled cuvette (Height: 42.5 mm, Width: 10 mm, Length: 20 mm), was used to create a deep, liquid pool and was the impact surface of the droplet. The free surface level was kept approximately constant by the cuvette overflowing. The experiments were carried out at 25°C and atmospheric pressure in the chamber. To avoid surfactant contamination for the water experiment, the system was prewashed with distilled water and fresh distilled water was used when the liquid container was emptied.

Droplet information such as cross-sectional area and x and y coordinates was processed using the ImageJ software (Abramoff et al., 2004). A custom script was used to analyze the data to determine the droplet diameter, impinging and bouncing velocities, and impinging angle. The estimated uncertainties of the diameter and velocity were 3 and 5 percent, respectively. These uncertainties propagated to the dimensionless parameters, the Weber number and Ohnesorge number ($\mathrm{Oh} = \frac{\mu}{\sqrt{\rho D \sigma}}$, showing the relative importance of the viscosity (μ) to surface tension), which had been typically used to characterize the regime-thresholds in the droplet impact. The

[5]For a 0.2–0.3 mm diameter bouncing drop, as will be seen later, the contact time is about 1 ms. Thus, a 125 Hz frequency allows for 7 'contact times' between each impact, which according to our observations, was enough for the surface to calm down. Further, the waves generated at the bouncing transitions are minor.

uncertainty in the Weber number and Ohnesorge number was thus estimated to be less than 8 percent.

3. Experimental observations

The regimes of coalescence and bouncing are schematically illustrated in Figure 2. In the

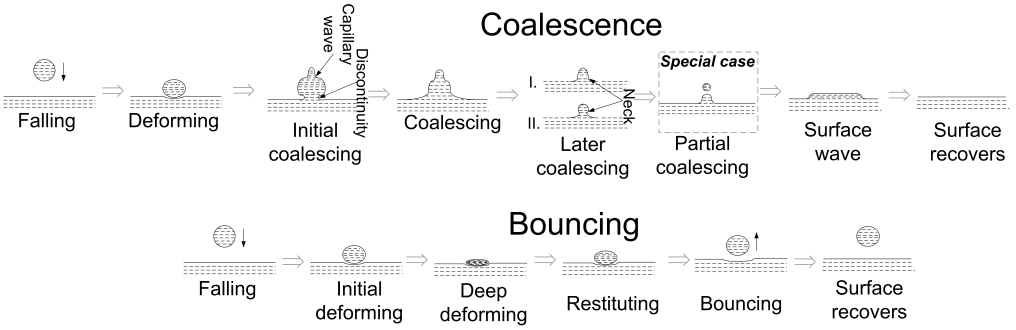

Figure 2: Schematic drawing of coalescence and bouncing.

coalescence regime, the impinging droplet merges into the liquid pool due to the film drainage either by the inertial force (high-energy-collision coalescence) or by the molecular/Van der Waals force (low-energy-collision coalescence) (Zhbankova and Kolpakov, 1990). In a special case, a part of the droplet can pinch off. During the merging process, as shown in Figure 2, a discontinuity is formed at the interface, where the impinging droplet hits the pool surface, and in the later merging stage (step 4), a neck, either thick (case I) or thin (case II), is formed. In the pinch-off process, the thin neck may rupture due to the delay of the vertical collapse of the neck compared to the horizontal collapse (Blanchette and Bigioni, 2006).

In the bouncing regime, as shown in Figure 2, both the droplet and pool surface undergo deformation during the period that they are in contact. After the maximum deformation, the droplet restitutes and bounces off the surface. The impinging angle is defined as the acute angle ($\leq 90°$) formed by the trajectory of an impinging droplet and the horizontal liquid surface, and an impinging angle of 90° denotes a perpendicular impingement.

It has been recognized that the droplets' not coalescing is due to an interfacial gas film (Bradley and Stow, 1978; Zhbankova and Kolpakov, 1990). Bradley and Stow (1978) predicted theoretically the minimum thickness of the intervening gas film, below which coalescence occurs, for two approaching droplets. For two water droplets with radii less than 1 mm, the minimum thickness was found to be between 0.25 and 0.30 μm. Due to the fact that the image resolution of the present study was 6 μm/pixel, which was much greater than the minimum thickness, the drainage process and the gas film thickness could not be studied in sufficient detail. Another fact that made an experimental investigation of the intervening gas film difficult was that the contact interface could not be observed clearly due to the deformation of both the droplet and liquid surface.

Figure 3(a) and (b) show the sequential pictures of low-energy-collision coalescence (with lower impinging velocity than that in bouncing at the same diameter) and partial coalescence, respectively. These two flow regimes are associated with very low impinging kinetic energy. The surface waves caused by the impingement of these two flow regimes are minor, and they

disappear quickly (within 1–2 frames, approximately 0.1–0.2 ms) after the primary impinging droplet's merging into the liquid pool. This implies that the kinetic energy of the impinging droplet is quite low and dissipates fast due to viscous loss in the liquid phase.

$t = 0$ ms $t = 0.4340$ ms $t = 0.5425$ ms $t = 0.6510$ ms $t = 0.7595$ ms

(a) Low-energy-collision coalescence.

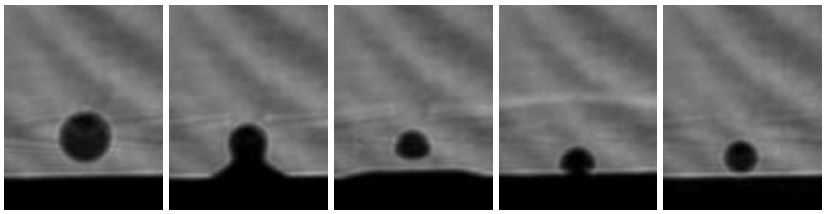

$t = 0$ ms $t = 0.7595$ ms $t = 0.8681$ ms $t = 0.9766$ ms $t = 1.3021$ ms

(b) Special case: partial coalescence

Figure 3: (a) Low-energy-collision coalescence: Low impact energy, small and subtle wave. Distilled water droplet: diameter $D = 0.11$ mm, velocity $V = 0.17$ m/s, impinging angle 86.5°. (b) Partial coalescence: distilled water droplet: diameter $D = 0.18$ mm, velocity $V = 0.29$ m/s, impinging angle 87.2°; bouncing diameter $D_b = 0.12$ mm, bouncing velocity $V = -0.26$ m/s, bouncing angle 89.0°.

Compared to low-energy-collision coalescence and partial coalescence, high-energy-collision coalescence can occur with higher impinging energy, and the impingement can cause stronger surface waves such as shown in Figure 4. Strong, expanding waves can be observed, and they last longer (more than 5 frames, approximately 0.6 ms) than the surface waves in low-energy-collision coalescence and partial bouncing. Some fringe patterns are visible in Figure 3(a) and (b) but not in Figure 4. This is because some of the pictures were taken using a monochromatic laser when the LED light was not available, and the laser gave interference fringes within its coherence length.

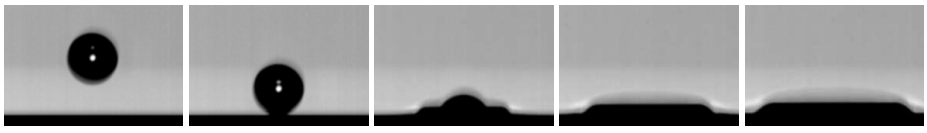

$t = 0$ ms $t = 0.1085$ ms $t = 0.2170$ ms $t = 0.3255$ ms $t = 0.4340$ ms

Figure 4: High-energy-collision coalescence: High impact energy, obvious and strong wave. 1-propanol droplet: diameter $D = 0.41$ mm, velocity $V = 2.3$ m/s, impinging angle 89.1°.

Bouncing is shown in Figure 5, the impinging droplet goes through deformation and resti-

tution without merging into the liquid pool, and there is momentum exchange but not mass exchange. The third image ($t = 0.3255$ ms) in Figure 5 shows that the impinging droplet looks like a flat pancake at around the highest deformation, and the restituting process after that is almost the reverse of the deforming process, except that the restituting droplet stretches longitudinally due to the up-going momentum. Considering the second image ($t = 0.2170$ ms) and fourth image ($t = 0.9766$ ms) of Figure 5, in which the droplet is at approximately the same position on its way downwards, and upwards, respectively, and the third image at the maximum deformation ($t = 0.3255$ ms), it can be seen that the restitution process is slower than the deformation process.

Figure 5: Bouncing: 1-propanol droplet: diameter $D = 0.24$ mm, velocity $V = 1.14$ m/s, impinging angle 89.8°; bouncing diameter $D_b = 0.24$ mm, bouncing velocity $V = -0.29$ m/s, bouncing angle 89.5°.

4. Results and discussion

4.1. Impinging and bouncing angle

This investigation focuses on close-to-perpendicular impacts. The impinging angle is plotted versus the bouncing angle in Figure 6 for the cases of bouncing and partial coalescence. Figure 6 shows the impinging and bouncing angles measured in a two-dimensional projection plane (x-z). The impinging angles are concentrated in the range of 85°–90°, while the according bouncing angles are more scattered. Approximately 94% of the impinging angles are in the range between 85° and 90°, and only 76% of the bouncing angles, excluding the case of partial coalescence, reach this level. In the case of partial coalescence, there are even fewer ($\approx 51\%$) bouncing angles above 85°. This indicates that the impingement is nearly vertical to the horizontal surface. However, the bouncing angles away from the vertical direction were affected by factors such as (1) a three-dimensional impingement trajectory and (2) the liquid surface deviating from perfectly flat and horizontal.

The three-dimensional impingement trajectory can be resolved by obtaining synchronized images from both projection planes, x-z and y-z. One camera was used in this investigation, as we expect the trajectory to lie in a plane. Another camera was, however, not available.

Regarding the liquid surface, in a few cases with high impinging frequencies (> 125 Hz), there were minor oscillations on the surface which could affect the bouncing trajectory. This was especially the case for partial coalescence, in which the secondary drop (pinch-off) impinged in a short time (a bit more than the contact time of approximately 1 ms, equivalent to 1000 Hz, for a $0.2 - 0.3$ mm impinging drop, see Section 4.3. See also Figure 3(b), the interval about 1 ms) after the primary droplet had impacted.

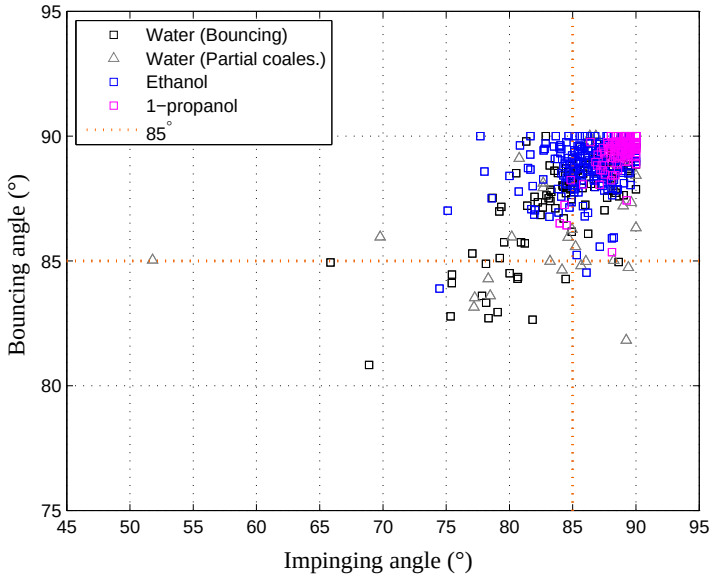

Figure 6: Impinging angle versus bouncing angle.

4.2. Characterization of flow regimes by velocity-diameter diagram

Figures 7(a), (c) and (e) show impinging velocity versus droplet diameter (*V*-*D*), and Figures 7(b), (d) and (f) show the Weber number versus the Ohnesorge number (We-Oh) for distilled water, technical ethanol and 1-propanol, respectively. The *V*-*D* diagrams of distilled water and ethanol show that low-energy-collision coalescence can be found below a certain diameter limit of around 0.2 mm, which will be discussed specifically in Section 4.2.1.

The We-Oh diagrams show that the transitions between the high-energy-collision coalescence and bouncing (C-B) are located at nearly constant Weber numbers, which, however, vary between fluids, and thus a generalized model is needed and will be presented in Section 4.5. Due to the diameter limit, the transitions to low-energy-collision coalescence (B-C) are found to be above certain levels of Ohnesorge number, Oh > 0.008 for water and Oh > 0.03 for ethanol.

4.2.1. Transition between coalescence and bouncing

Low-energy-collision coalescence, which occurs at a lower impinging velocity than that of bouncing at a fixed diameter, can occur for impinging droplets with diameters below a specific limit. Thus, in this region, bouncing is located between the high- and low-energy type coalescence, and there are correspondingly two transitions, coalescence-bouncing-coalescence (C-B-C), with collision energy from high to low. Above the diameter limit, only one transition, coalescence-bouncing (C-B), can be found. For the transition to low-collision-energy coalescence, B-C, there exists a cutoff, $\frac{1}{\mathrm{Oh}} = \frac{\sqrt{\rho D_{\mathrm{limit}} \sigma}}{\mu}$, which governs the competing effects from the surface tension and viscosity. Bouncing is inhibited, i.e. low-collision-energy coalescence dominates, when the diameter of a droplet becomes sufficiently small and the damping effects from viscosity are influential (Thoroddsen and Takehara, 2000).

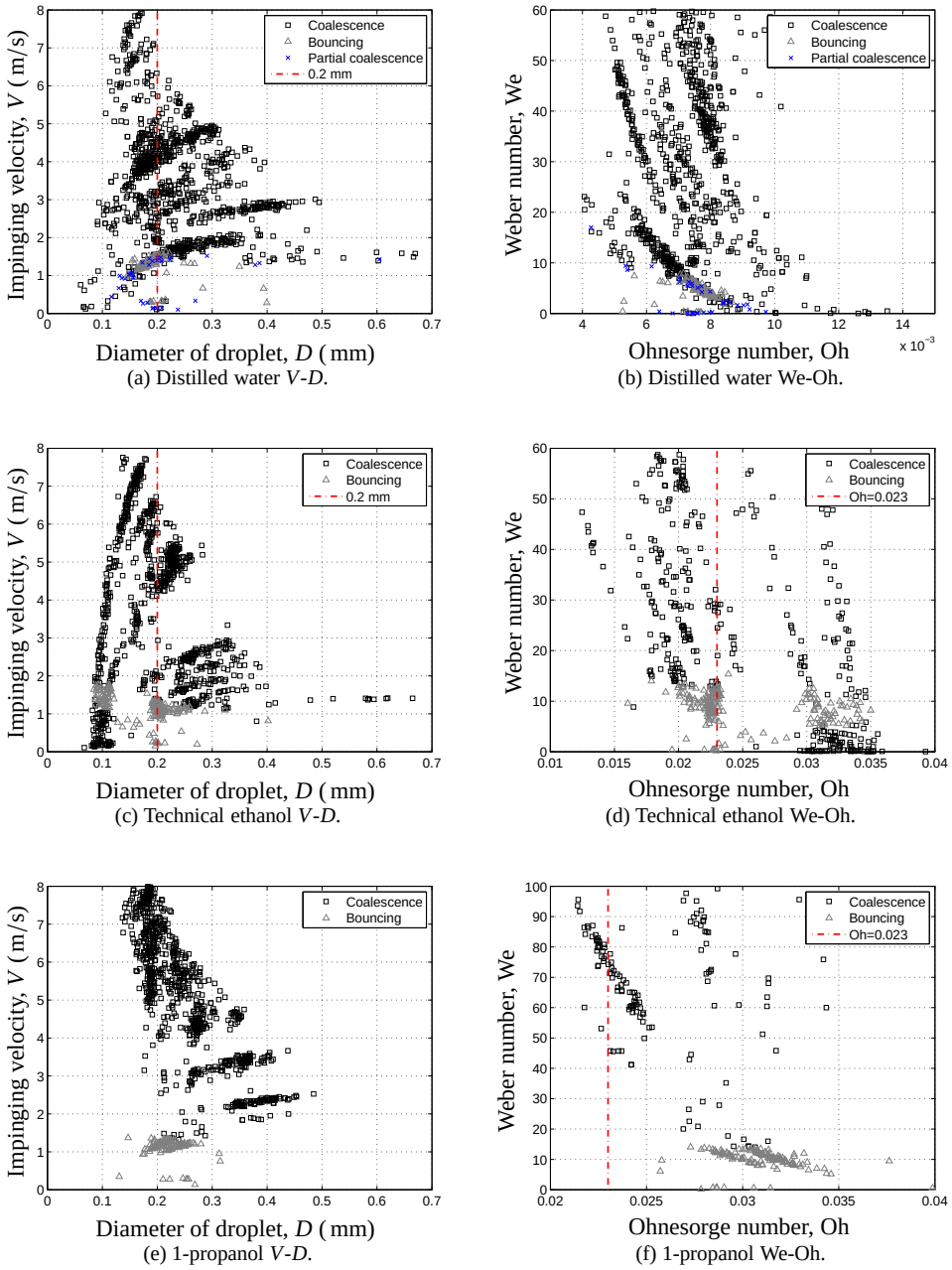

Figure 7: (a), (c) and (e): Impinging velocity against diameter of droplet. (b), (d) and (f): Weber number against Ohnesorge number for impinging droplet.

The diameter limit is found to be around 0.2 mm such as shown in Figure 7(a) and (c). No limit is shown for 1-propanol in Figure 7(e) due to an insufficient number of coalescence data points with low impact velocities (below 1 m/s). However, the diameter limit, $D = 0.2$ mm, gives different values for the cutoffs ($\frac{1}{\mathrm{Oh}} \approx 135$ for water and 45 for ethanol), which indicates that a more complete model including effects from inertia is needed for characterizing the threshold, and such a model is presented in Section 4.5.

4.2.2. Partial coalescence

With the breaking of the neck, which is shown in Figure 2 and Figure 3(b), partial coalescence occurs. It can be seen in Figure 7(a) that partial coalescence is distributed both above and below bouncing, as it is a transitional regime between bouncing and coalescence. Due to the low impinging velocity for bouncing and partial coalescence, measurement uncertainties can evidently affect the position of the data points on the figure, and it leads to the mixing-up of a part of the partial coalescence data with the bouncing data.

Partial coalescence is only found in the experiments with distilled water, and this can be qualitatively explained by the competing effects from the viscosity and surface tension. According to Blanchette and Bigioni (2006), high viscosity can inhibit the capillary waves which act to stretch the drop and delay the vertical collapse, and thus restrain the neck rupture that lead to partial coalescence. On the other hand, the fact that Blanchette and Bigioni (2006) found that partial coalescence was suppressed at high Ohnesorge numbers can also indicate that partial coalescence is promoted by surface tension (low Ohnesorge numbers).

A quantitative explanation for the inhibition of partial coalescence in the experiments of ethanol and 1-propanol is that there exists an Ohnesorge-number limit (Blanchette and Bigioni, 2006; Zhang et al., 2009), above which the pinch-off of a droplet does not occur, i.e. partial coalescence is completely inhibited. The Ohnesorge-number limit suggested by the simulation of Blanchette and Bigioni (2006) was 0.026, and Zhang et al. (2009) pointed out that this limit should be 0.023–0.026 for a drop impacting on a flat liquid surface. Figure 7(d) and (f) show that most of the experimental data of ethanol and 1-propanol is above the limit $\mathrm{Oh} = 0.023$, and this corresponds to a complete inhibition of partial coalescence. Below the limit, no experimental data is available for 1-propanol with low enough impact Weber number (Zhang et al. (2009) used $\mathrm{We} = 1$ for water and glycerin mixture), and for the experimental data of ethanol, there are only a few (about 5) data points with low impact Weber number ($\mathrm{We} < 5$). Thus, it can be concluded that the present investigation of ethanol and 1-propanol contain very few data points for $\mathrm{Oh} < 0.023$ with suitably low impact Weber number for partial coalescence.

Zhang et al. (2009) identified a novel type "second-stage" partial coalescence, which had a smaller diameter ratio between bouncing and impinging droplet ($\frac{D_b}{D} \approx 0.2$) than the "first-stage" ($\frac{D_b}{D} \approx 0.5$). Here, the "second-stage" partial coalescence was not observable due to, (1) most of the droplet diameters for partial coalescence in the present investigation were below 0.3 mm (see Figure 8(a)), thus corresponding to a shorter interaction time (≈ 1 ms, see Figure 3(b)) than that if about 10 ms for the illustrative images in Zhang et al. (2009), and (2) the camera speed in this study was about 10000 fps, which was lower than the speed of up to 60000 fps in Zhang et al. (2009). However, Figure 8 shows that there are also two levels of the diameter ratio ($\frac{D_b}{D} \approx 0.65$ and 0.42), which may indicate the similar first- and second-stage partial coalescence, respectively. Perhaps due to the higher impinging Weber numbers in the present study, the diameter ratios are higher than those of ≈ 0.5 and 0.2 in Zhang et al. (2009).

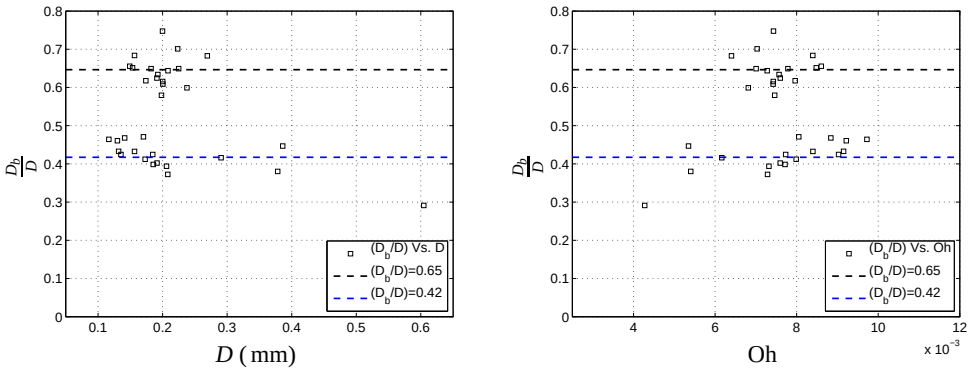

(a) Diameter ratio against D.

(b) Diameter ratio against Oh.

Figure 8: The bouncing-impinging diameter ratio ($\frac{D_b}{D}$) for partial coalescence. (a) Against impinging diameter. (b) Against impinging Ohnesorge number.

4.3. Contact time

One important parameter for the investigation of bouncing is the contact time, between which an impinging droplet interacts with a target, a liquid surface in the present study. The high-speed camera operating at nearly 10^4 Hz enables the measurement of contact time with limited errors.

In Figure 9(a), the contact time is investigated as a function of the impinging velocity, and this investigation is carried out with a fixed diameter at 0.22 ± 0.004 mm. The contact time shows little dependence on the impinging velocity, and this agrees well with Richard et al. (2002), despite different fluids and targets considered in Richard et al. (2002) (water and a dry surface) and in this investigation (1-propanol and a liquid surface). A droplet with a lower impinging velocity (0.28 m/s) than the others deviates more from the constant contact time ($\approx$ 1 ms), and this is due to overestimation. The reason is that the contact line on a liquid surface cannot be sharply defined due to the liquid surface deformation, and so, the moment of visual detection for the detachment between the rebound drop and surface is always a little delayed with respect to the exact moment of the detachment. The overestimation becomes considerable for a droplet with a small bouncing velocity, as it takes a long time for the rebound drop to reach a region where a clear separation between the drop and surface can be observed.

There exists an inherent bouncing time scale,

$$\tau^* = \sqrt{\frac{\rho D^3}{\sigma}}, \tag{1}$$

for bouncing of a droplet on both a liquid surface (Thoroddsen and Takehara, 2000, partial coalescence, strictly speaking) and a dry surface (Richard et al., 2002). As Figure 9(a) indicates that the contact time is independent of the velocity, we could examine the relation between contact time and diameter using different velocities. Figure 9(b) shows the contact time (τ) against the diameter (D) in a log-log coordinate system. Still, in Figure 9(b), most of the data points have the same impinging velocity (1.20 ± 0.04 m/s), except for the two larger droplets at $D \approx 0.31$ mm ($V = 0.75$ and 0.95 m/s) and two smaller droplets at $D \approx 0.14$ mm ($V = 0.35$ and 1.37 m/s).

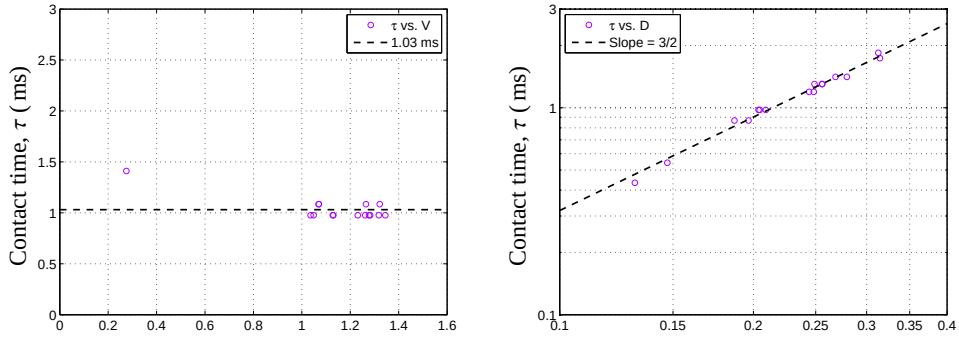

(a) Fixed droplet diameter. (b) Varying droplet diameter.

Figure 9: (a) Contact time (τ) versus droplet impinging velocity (V) with the impinging droplet diameter fixed at 0.22 mm, using 1-propanol. (b) Log-log plot of contact time (τ) versus droplet diameter (D), using 1-propanol. The droplets have a velocity of 1.2 m/s, except for the two larger droplets at $D \approx 0.31$ mm ($V = 0.75$ and 0.95 m/s) and two smaller droplets at $D \approx 0.14$ mm ($V = 0.35$ and 1.37 m/s).

Figure 9(b) exhibits that the contact time is dependent on the droplet diameter, and it fits well with the time scale τ^* as shown by the slope of $\frac{3}{2}$ in log-log coordinate system, which agrees with Thoroddsen and Takehara (2000); Richard et al. (2002). Thus the contact time (τ) can be expressed as follows

$$\tau = C \cdot \tau^* = C \cdot \sqrt{\frac{\rho D^3}{\sigma}}, \tag{2}$$

where $C = 1.72$ is a prefactor of the time scale and is determined by using least-squares regression.

4.4. Restitution coefficient

The restitution coefficient ($\epsilon = \frac{|V_b|}{|V|}$) is defined by the ratio between the absolute value of the bouncing velocity ($|V_b|$) and the absolute value of the impinging velocity ($|V|$), and it can be used to study the kinetic-energy loss of the impinging droplet during its interaction with the liquid surface. In Figure 10, the restitution coefficient is plotted versus the Weber number for impinging droplets. As can be seen from Figure 10, the restitution coefficient is relatively high when the impinging Weber number is low, and this means that the inertial energy is well preserved in the form of elastic potential energy related to droplet and pool surface deformation during the impingement. As the Weber number increases, the restitution coefficient drops rapidly to a relatively stable level, where for each fluid the restitution coefficient varies within the range of approximately 0.2–0.3 with a maximum fluctuation around ±0.025, as shown in Figure 10. The experimental data on the restitution coefficient agrees well with Bach et al. (2004); Jayaratne and Mason (1964).

The dramatic decrease in the restitution coefficient around We = 1 is a non-ideal character in bouncing, and according to Richard and Quéré (2000) for droplet-dry-surface impingement, the dissipation processes are more obvious as the impinging kinetic energy increases due to more

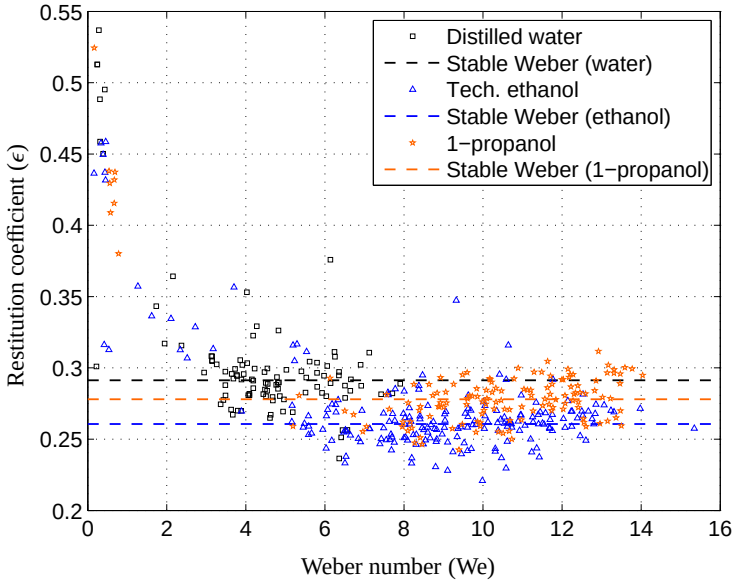

Figure 10: The restitution coefficients for the impact of a droplet with a deep liquid pool versus the Weber number. The stable Weber numbers are the averaged values in stable ranges.

oscillations of the droplets. For droplet-liquid-surface impingement, at high Weber numbers, a larger portion of the impinging kinetic energy is transformed into the energy forms related to the oscillations of both liquid surface (waves) and droplet, and it is finally dissipated (Bach et al., 2004).

Table 2 lists the stable restitution coefficients, which are calculated by averaging the restitution coefficients within the stable range (median value ±0.025), and in spite of different experimental fluids, the stable restitution coefficients are relatively close. The assumption is that, in bouncing, the ratio of energy loss into the oscillation of the pool surface and capillary waves, is similar for different cases where the impinging Weber number is higher than 1, and thus leads to the similar stable level of restitution coefficient. The stable restitution coefficients, however, vary somewhat, and this indicates that the physical properties affect the bouncing process.

Table 2: Stable level of the restitution coefficient.

Fluid	Stable restitution coefficient
Distilled water	0.29
Technical ethanol	0.26
1-propanol	0.28

The effects of the physical properties on the stable level restitution coefficient are discussed in Section 4.4.1 and 4.4.2. The spreading of restitution coefficients at a fixed Weber number (see

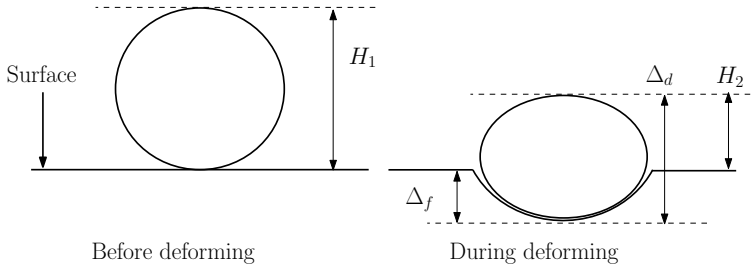

Figure 11: Schematic drawing of the deformation process of a droplet on a liquid surface.

Figure 10) is assumed to be as a result of different kinematic parameters, and it is discussed in Section 4.4.3.

4.4.1. Effects of viscosity

Technical ethanol and 1-propanol have quite similar densities ($\approx$ 800 kg/m^3) and surface tensions (22 mN/m), and 1-propanol, with about 50% higher viscosity than technical ethanol (see Table 1), gives a higher restitution coefficient. This conclusion seems to be contrary to the common recognition that higher viscosity corresponds to more viscous dissipation, i.e. lower restitution coefficient, but this is true only with a prerequisite that the droplets and liquid surfaces in both bouncing cases undergo the same deformation process with approximately the same surface tension. The deformation process of a droplet on a liquid surface is different from that on a solid surface (Richard and Quéré, 2000; Richard et al., 2002; Clanet et al., 2004, etc.), in which a partial no-slip condition is considered.

Figure 11 schematically shows the deformation process. Right before deforming, the droplet diameter is the same as the height from the top of the droplet to the surface (H_1). During deforming, the surface sinks with a value of Δ_f, and the minor axis of the droplet becomes Δ_d due to the deformation. Similar to the function of a spring, the elastic potential energy is conserved in the deformation of both the droplet (denoted by $H_1 - \Delta_d$) and the surface (Δ_f), and thus the elastic potential energy can be indicated by the height difference between the two different stages during the deformation process as $H_1 - \Delta_d + \Delta_f = H_1 - H_2$. Thus, the height of the droplet, from the top of the droplet to the initial undisturbed surface, is investigated and shown in Figure 12, in which two pairs of bouncing processes from ethanol and 1-propanol with the same impinging parameters (diameter and velocity) are compared. The two pairs show a similar trend of height-variations for ethanol and 1-propanol.

One remarkable fact is that the maximum deformation is reached in both cases by approximately the same time (0.2 ms), while the 1-propanol droplet is more flattened at the maximal deformation. After nearly the same oscillation period (0.5 ms), during which the droplet and liquid surface undergo different restitution paces, the droplet starts restoring with a steady increase in height. Figure 12 shows that the restituting processes for ethanol and 1-propanol also take approximately the same time (0.4 ms), and this is indicated by Eq. (1), showing that the contact time for ethanol and 1-propanol droplets of the same size should be nearly the same[6]. With approximately the same surface tension, the higher deformation for the higher-viscosity fluid, leads to,

[6]restituting time = contact time – deforming time – oscillating time. In fact, the restituting time for the 1-propanol droplet should be slightly less than for ethanol by Eq. (1) given the same diameter, while this is not shown by Fig. 12 due to the uncertainty of the exact moment for the drop-film detachment.

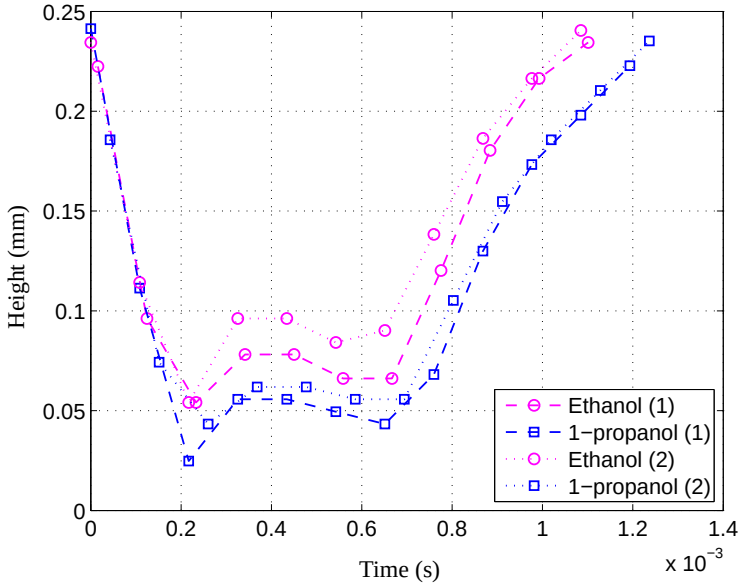

Figure 12: Two realizations showing the deformed droplet (puddle) heights of an ethanol droplet ($\mu = 1.367\,\mathrm{mPa\cdot s}$) and a 1-propanol droplet ($\mu = 1.968\,\mathrm{mPa\cdot s}$) with the same kinematic parameters, $D = 0.25\,\mathrm{mm}$, $V = 1.19\,\mathrm{m/s}$ for pair (1), $D = 0.25\,\mathrm{mm}$, $V \approx 1.13\,\mathrm{m/s}$ for pair (2).

on one side, more viscous loss, while on the other side, conserves more kinetic energy. Overall, the energy difference between the elastic potential energy (preserved at the maximal deformation) and the viscous loss (during the whole deformation) for the high-viscosity fluid prevails that for the low-viscosity fluid, and thus higher velocity can be recovered (with two fluids of nearly the same density and surface tension). Another way to understand the higher bouncing velocity of the 1-propanol droplet is that, through the same restituting time, more distance, corresponding to the higher maximal deformation, is traveled.

4.4.2. Effects of surface tension

Using the above conclusion on the effects of viscosity during bouncing, distilled water with a lower viscosity than technical ethanol and 1-propanol is expected to have a lower stable restitution coefficient, while on the contrary, it has a higher stable restitution coefficient. This indicates that the effects from density and surface tension are also significant. Compared with the surface tension, the densities of distilled water, ethanol and 1-propanol are considered to be close, and thus the high surface tension of distilled water promotes the restitution coefficient.

4.4.3. Effects of kinematic parameters

Figure 10 also shows that different restitution coefficients can be found at a fixed Weber number, especially in the stable region. The reason is that the droplets with the same Weber number can correspond to different diameters, and so different impinging velocities (see the We-Oh diagram in Figure 7(a), (c) and (e), in which Oh is solely dependent on D for a certain fluid). The differences in diameter and velocity can lead to different portions of loss in the kinetic

energy, due to, for instance, different contact times as shown in Section 4.3, and thus different restitution coefficients can be found at a fixed Weber number. Furthermore, although they are not assumed to be dominant here, the surface conditions, in which a slight change of angle or small waves and oscillations can affect the bouncing velocity, may also lead to a fixed Weber number corresponding to multiple restitution coefficients.

4.5. Characterization of flow regimes by a We-Oh *correlation*

In this section, an attempt is made to generalize a correlation to characterize the transitions between bouncing and coalescence.

The transitions between the flow regimes, which are associated with relatively high inertia collision, such as the transitions between coalescence and splashing/jetting, are commonly characterized using correlations sharing the same form (Cossali et al., 1997; Mundo et al., 1995)

$$\mathrm{We} \cdot \mathrm{Oh}^{a} = b, \tag{3}$$

and Zhao et al. (2011) listed some of the values of a and b used in the investigations for the high inertia collision. There are, however, very few investigations dealing with the characterization of the transitions between the flow regimes associated with relatively low inertia collisions, such as the transitions between coalescence and bouncing. Huang and Zhang (2008) characterized the transition between high-energy-collision coalescence and bouncing (C-B) with $\mathrm{We}^{0.375} \cdot \mathrm{Re}^{0.25} = 13$, which can be rewritten as $\mathrm{We} \cdot \mathrm{Oh}^{-0.5} = 169$, using the relation $\mathrm{Re} = \sqrt{\mathrm{We}}/\mathrm{Oh}$. We found that this correlation overestimated the C-B threshold with the data reported in the present investigation.

A generalized correlation for the transitions between both the high-energy-collision and low-energy-collision coalescence and bouncing was found by employing the approach outlined by Zhao et al. (2011). Herein, a threshold line is characterized with the least number of uncertain points[7]. For the threshold of high-energy-collision coalescence and bouncing (C-B), a trial and error method was employed for finding the parameters, a and b, in Eq. (3) with a in the range $[-0.7, -0.1]$ with a step of 0.01 and b in the range $[0, 200]$ with a step of 1.[8] For the threshold of bouncing and low-energy-collision coalescence (B-C), this trial and error method searched for the parameter b in the range $[0, 80]$ with a step of 1, while it kept the same exponent found for the C-B threshold. It must be pointed out that, due to the fact that the coalescence data were distributed both below and above the bouncing data, ranges of the Weber number and Ohnesorge number for separating the high-energy-collision coalescence and low-energy-collision coalescence were given to ensure that the trial and error method returned the solution using the reasonable We and Oh ranges.[9]

[7] Uncertain points: The data points of one regime found in a range where the majority of points are from another regime.

[8] A certain compromise must be made due to the fact that the best solution, which gave the least number of uncertain points, for an experimental fluid was always different from the best solution for another fluid, and thus we used the solution that gave the minimum sum of squares of the numbers of uncertain points for all fluids.

[9] To identify high-energy-collision coalescence, We > 6.7 for water, We > 12.4 for ethanol, We > 14.0 for 1-propanol was used, and to identify low-energy-collision coalescence, both the Weber number and Ohnesorge number must be given, Oh > 0.008 &We < 2.8 for water, Oh > 0.03 & We < 5.9 for ethanol was used. The above limits for the Weber numbers characterized the C-B and B-C thresholds (Zhao, 2009), and the limits for the Ohnesorge numbers were found as approximately the lowest Ohnesorge number where the low-energy-collision coalescence appeared (Zhao, 2009, see also Section 4.2, Figures 7(a) and (c)).

This gave the following correlation for the transitions between the high-energy-collision and low-energy-collision coalescence and bouncing:

$$K = \mathrm{We} \cdot \mathrm{Oh}^{-0.58} \begin{cases} K = 119 & \text{(for C-B threshold)} \\ K = 43 & \text{(for B-C threshold),} \end{cases} \tag{4}$$

where the exponent (-0.58) in Eq. (4) is close to the exponent (-0.57) for coalescence and jetting threshold found by Zhao et al. (2011).

Figure 13(a) shows the We-Re diagram with logarithmic coordinates, where the thresholds characterized using Eq. (4) and a C-B threshold correlation (Huang and Zhang, 2008) are plotted. Figure 13(b) shows a close-up at the regime transitions, where the overlap of bouncing and coalescence is difficult to identify in Figure 13(a).

There are several remarkable facts:

- Agreement with the experimental results both from the present study and the literature (Huang and Zhang, 2008): Figure 13(a) shows that, for the experimental data in the present study, both the C-B and B-C thresholds can be well characterized by the correlation (4), and the model by Huang and Zhang (2008) characterizes a higher C-B threshold. Both correlations are also compared with the experimental data of Huang and Zhang (2008) using oil, for which the viscosity ($23\,\mathrm{mPa \cdot s}$) is approximately 20 times that of water and ethanol but with a comparable surface tension ($29\,\mathrm{mN/s}$) to the alcohols. Even though Eq. (4) predicts a lower threshold than the Huang and Zhang (2008) correlation, Eq. (4) is believed to work as well in characterizing the C-B threshold for oil due to the C-B transition uncertainty, as the transition chosen by Huang and Zhang (2008) is not absolutely certain (coalescence is found between bouncing) and the Eq. (4) fits on this uncertain part.

- Partial coalescence: The partial coalescence data from distilled water are found to be scattered in both the coalescence and bouncing regimes, while many of them are in the vicinity of the C-B and B-C thresholds by Eq. (4).

- Uncertainty in the transitions: Some data points are characterized into the "wrong" regimes by the correlation (4). The number of these data points are found to be small ($\approx$ 40 for all fluids at the C-B threshold[10]) with respect to the large number ($\approx$ 3000 for all fluids) of high-energy-collision coalescence and bouncing data. For the B-C threshold, there seems to be a larger overlapping part between bouncing and coalescence than that at the C-B threshold. The main reason is that the low-energy-collision coalescence exists only below a diameter limit (0.2 mm, see Section 4.2), while above this limit, bouncing points are predominantly found, but they can have similar values for the Weber and Reynolds numbers as some of the low-energy-coalescence points.

5. Concluding remarks

This investigation studied vertical impingement of droplets on a deep pool with focus on the flow regimes of high- and low-energy-collision coalescence, partial coalescence and bouncing. Velocity-diameter (V–D) diagrams showed that low-energy-collision coalescence existed below

[10]This is approximate number due to the fact that the coalescence must be manually defined as high- and low-energy-collision coalescence according to the Weber number before the data treatment, and thus an uncertainty exists.

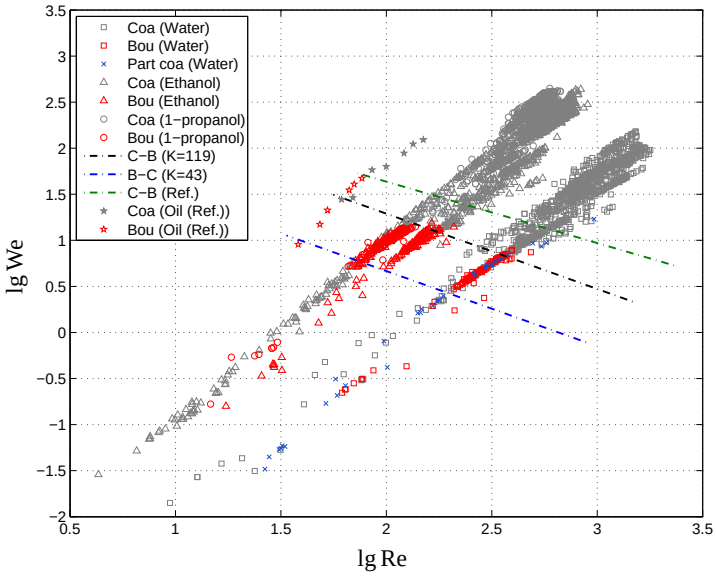

(a) lg We-lg Re, overview.

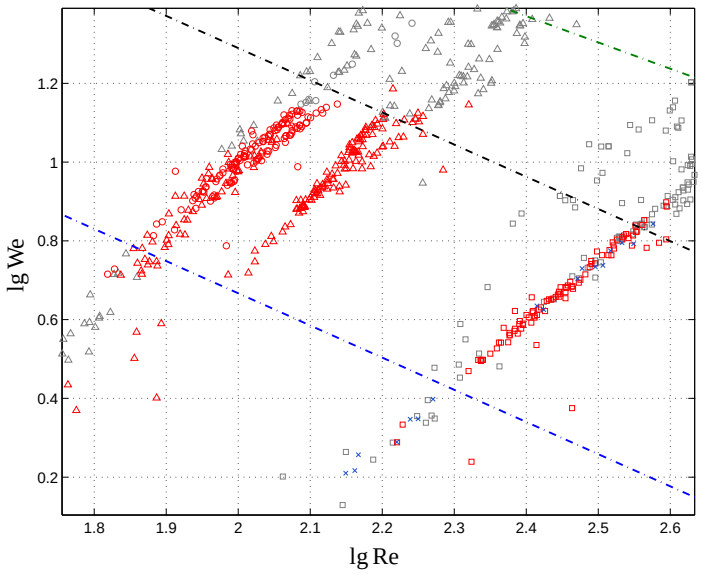

(b) lg We-lg Re, close-up around regime-transitions.

Figure 13: The logarithmic We-Re diagram for coalescence and bouncing of droplets. The legends marked with Ref. is from Huang and Zhang (2008). (a) overview and (b) close-up around regime-transitions.

a diameter limit ($D \approx 0.2$ mm). Partial coalescence was only observed with the experiments using distilled water but not ethanol and 1-propanol, and this was attributed to the effects from the high viscosities and low surface tensions of the alcohols compared with water, which weakened the conditions for the neck rupture. The suppression of partial coalescence in the experiments of ethanol and 1-propanol was expected to occur with the Ohnesorge number above 0.023, which agreed well with Blanchette and Bigioni (2006); Zhang et al. (2009). The contact time of the 1-propanol droplet showed little dependence on the droplet impinging velocity. Instead, it was dependent on the droplet diameter, and it fitted well the bouncing time scale τ^* with a prefactor 1.72.

The stable restitution coefficient was in the range 0.26–0.29, in which the water data agreed well with other results (Bach et al., 2004; Jayaratne and Mason, 1964). Increased viscosity and surface tension resulted in an elevated restitution coefficient, and thus promoted the bouncing velocity. Correlation (4) ($K = \mathrm{We} \cdot \mathrm{Oh}^{-0.58}$) was employed for characterizing both the C-B and B-C thresholds, and it agreed well with the experimental results from both the present study and the literature (Huang and Zhang, 2008).

Acknowledgements

This publication forms a part of the Remote Gas project, performed under the strategic Norwegian research programme Petromaks. The authors acknowledge the partners; Statoil, UOP, Bayerngas Norge, Aker Solutions, DNV, and the Research Council of Norway (168223/S30) for support. The reporting was supported by the Enabling Low-Emission LNG Systems project, and the authors acknowledge the contributions of GDF SUEZ, Statoil and the Petromaks programme of the Research Council of Norway (193062/S60). He Zhao wishes to express his gratitude to his PhD supervisor, Jostein Pettersen (Adjunct Professor at NTNU and project leader at Statoil). Thanks are due to Senior Engineer Håvard Rekstad at NTNU for making the test-cell drawings.

Thanks are due to the anonymous reviewers for their constructive remarks, which lead to substantial improvements of the first versions of this paper.

Abramoff, M. D., Magelhaes, P. J., Ram, S. J., 2004. Image processing with imagej. Biophotonics Int. 11 (7), 36–42.
Austrheim, T., 2006. Experimental Characterization of High-Pressure Natural Gas Scrubbers. Ph.D. thesis, University of Bergen.
Aziz, S. D., Chandra, S., 2000. Impact, recoil and splashing of molten metal droplets. Int. J. Heat Mass Transfer 43 (16), 2841–2857.
Bach, G. A., Koch, D. L., Gopinath, A., 2004. Coalescence and bouncing of small aerosol droplets. J. Fluid Mech. 518, 157–185.
Bartolo, D., Bouamrirene, F., Verneuil, E., Buguin, A., Silberzan, P., Moulinet, S., 2006. Bouncing or sticky droplet: impalement transitions on superhydrophobic micropatterned surface. Europhys. Lett. 74 (2), 299–305.
Blanchette, F., Bigioni, T. P., April 2006. Partial coalescence of drops at liquid interfaces. Nat. Phys. 2, 254–257.
Bradley, S. G., Stow, C. D., 1978. Collisions between liquid drops. Philos. Trans. R. Soc. London, Ser. A 287 (1349), 635–675.
Brunet, P., Lapierre, F., Thomy, V., Coffinier, Y., Boukherroub, R., 2008. Extreme resistance of superhydrophobic surfaces to impalement: reversible electrowetting related to the impacting/bouncing drop test. Langmuir 24 (19), 11203–11208.
Clanet, C., Béguin, C., Richard, D., Quéré, D., 2004. Maximal deformation of an impacting drop. J. Fluid Mech. 517, 199–208.
Cossali, G. E., Coghe, A., Marengo, M., 1997. The impact of a single drop on a wetted solid surface. Exp. Fluids 22, 463–472.
Couder, Y., Fort, E., Gautier, C. H., Boudaoud, A., 2005. From bouncing to floating: noncoalescence of drops on a fluid bath. Phys. Rev. Lett. 94, 177801.
Deng, T., Varanasi, K. K., Hsu, M., Bhate, N., Keimel, C., Stein, J., Blohm, M., 2009. Nonwetting of impinging droplets on textured surfaces. Appl. Phys. Lett. 94 (13), 133109.
Dorao, C. A., Fernandino, M., Patruno, L. E., Dupuy, P. M., Jakobsen, H. A., Svendsen, H. F., 2009. Macroscopic description of droplet-film interaction for gas-liquid systems. Appl. Math. Model. 33 (8), 3309–3318.
Dupuy, P. M., Kleinohl, N., Fernandino, M., Jakobsen, H. A., Svendsen, H. F., 2010. Droplet-surface impact at high pressures. Chem. Eng. Sci. 65, 5320–5343.
Huang, Q. Y., Zhang, H., 2008. A study of different fluid droplets impacting on a liquid film. Pet. Sci. 5, 62–66.
Jayaratne, O. W., Mason, B. J., 1964. The coalescence and bouncing of water drops at an air/water interface. Proc. R. Soc. London, Ser. A 280 (1383), 545–565.
Johnsen, C. G., 2007. Experimental and Numerical Investigation of Droplet Phenomena. Ph.D. thesis, Norwegian Univesity of Science and Technology.
Jung, Y. C., Bhushan, B., 2008. Dynamic effects of bouncing water droplets on superhydrophobic surfaces. Langmuir 24 (12), 6262–6269.
Jung, Y. C., Bhushan, B., 2009. Dynamic effects induced transition of droplets on biomimetic superhydrophobic surfaces. Langmuir 25 (16), 9208–9218.
Kwon, H.-M., Paxson, A. T., Varanasi, K. K., Patankar, N. A., Jan 2011. Rapid deceleration-driven wetting transition during pendant drop deposition on superhydrophobic surfaces. Phys. Rev. Lett. 106 (3), 036102.
Lide, D. R., 2009. CRC Handbook of Chemistry and Physics, 89th Edition. CRC Press.
Lord Rayleigh, F. R. S., 1878. On the instability of jets. Proc. London Math. Soc. 10, 4–13.
Lord Rayleigh, F. R. S., 1879. On the capillary phenomena of jets. Proc. R. Soc. London 29, 71–97.
Madden, L. V., 1997. Effects of rain on splash dispersal of fungal pathogens. Can. J. Plant. Pathol. 19, 225–230.
Mao, T., Kuhn, D. S., Tran, H., 1997. Spread and rebound of liquid droplets upon impact on flat surfaces. AlChE J. 43 (9), 2169–2179.
Moita, A. S., Moreira, A. L., 2007. Experimental study on fuel drop impacts onto rigid surfaces: Morphological comparisons, disintegration limits and secondary atomization. Proc. Combust. Inst. 31 (2), 2175–2183.
Mundo, C., Sommerfeld, M., Tropea, C., 1995. Droplet-wall collisions: Experimental studies of the deformation and breakup process. Int. J. Multiphase Flow 21 (2), 151–173.
Ohnuki, Y., Shimizu, A., 2004. Experimental studies on rain splash erosion of forest soils after clearing in okinawa using an artificial rainfall apparatus. J. For. Res. 9 (2), 101–109.
Pan, K. L., Law, C. K., 2007. Dynamics of droplet-film collision. J. Fluid Mech. 587, 1–22.
Pasandideh-Fard, M., Aziz, S. D., Chandra, S., Mostaghimi, J., 2001. Cooling effectiveness of a water drop impinging on a hot surface. Int. J. Heat Fluid Flow 22 (2), 201–210.
Richard, D., Clanet, C., Quéré, D., 2002. Surface phenomena: Contact time of a bouncing drop. Nature 417, 811.
Richard, D., Quéré, D., 2000. Bouncing water drops. Europhys. Lett. 50 (6), 769–775.
Rioboo, R., Voué, M., Vaillant, A., De Coninck, J., 2008. Drop impact on porous superhydrophobic polymer surfaces. Langmuir 24 (24), 14074–14077.
Schotland, R. M., 1960. Experimental results relating to the coalescence of water drops with water surfaces. Discuss. Faraday Soc. 30, 72–77.

Tanaka, Y., Matsuda, Y., Fujiwara, H., Kubota, H., Makita, T., 1987. Viscosity of (water + alcohol) mixtures under high pressure. Int. J. Thermophys. 8 (2), 147–163.

Thoroddsen, S. T., Takehara, K., 2000. The coalescence cascade of a drop. Phys. Fluids 12 (6), 1265–1267.

Tsai, P., Pacheco, S., Pirat, C., Lefferts, L., Lohse, D., 2009. Drop impact upon micro- and nanostructured superhydrophobic surfaces. Langmuir 25 (20), 12293–12298.

Tuck, C. R., Ellis, M. C. B., Miller, P. C. H., 1997. Techniques for measurement of droplet size and velocity distributions in agricultural sprays. Crop Prot. 16 (7), 619–628.

Vaquez, G., Alvarez, E., Navaza, J. M., 1995. Surface tension of alcohol + water from 20 to 50°c. J. Chem. Eng. Data 40, 611–614.

Worthington, A. M., 1876. On the forms assumed by drops of liquids falling vertically on a horizontal plate. Proc. R. Soc. London 25, 261–272.

Zhang, F. H., Li, E. Q., Thoroddsen, S. T., 2009. Satellite formation during coalescence of unequal size drops. Phys. Rev. Lett. 102 (10), 104502.

Zhao, H., 2009. An Experimental Investigation of Liquid Droplets Impinging Vertically on a Deep Liquid Pool. Ph.D. thesis, Norwegian University of Science and Technology.

Zhao, H., Brunsvold, A., Munkejord, S. T., 2011. Investigation of droplets impinging on a deep pool: transition from coalescence to jetting. Exp. Fluids 50 (3), 621–635.

Zhao, H., Brunsvold, A., Munkejord, S. T., Mølnvik, M. J., 2010. An experimental method for studying the discrete droplet impact phenomena in a flammable gas environment. J. Nat. Gas Sci. Eng. 2, 259–269.

Zhbankova, S. L., Kolpakov, A. V., 1990. Collision of water drops with a plane water surface. Fluid Dyn. 25 (3), 470–473.